KONURALP JOURNAL OF MATHEMATICS
VOLUME 3 NO. 2 PP. 1–16 (2015) ©KJM

EFFECT OF THE CAVITY ANGLE ON FLOW STRUCTURES IN AN ANNULAR WEDGE CAVITY

HALIS BILGIL, ZARIFE DOLEK

ABSTRACT. This paper analyzes the 2-D Stokes flow in annular wedge cavities with different cavity angles. In order to analyze the flow structures, the two dimensional biharmonic equation is solved analytically. The flow is governed by two physical control parameters: the cavity angle α and the ratio of the upper and lower lid speeds ($S = \frac{U_1}{U_2}$). By varying α for each S, the effect of cavity angle on the streamline patterns and their bifurcations are investigated.

1. INTRODUCTION

Stokes flow generated within different shaped cavities is encountered in several manufacturing processes and engineering applications. The list of some of these applications can be found in the references [6,12,14,17]. Flow within the cavities has also been a focus attention for computational fluid dynamic studies since it is a commonly used as a benchmark problem.

There are many works in the literature on cavity flows related to eddy structure and their bifurcations. Gürcan et al. [8] analyzed the generation of eddies in a rectangular cavity. They showed effects of cavity aspect ratio and speed ratio of the moving lids on the streamline topology and the flow bifurcations. Flow bifurcation and eddy generation for steady, viscous flow in an L-shaped cavity, with the lids moving in opposite directions, has been investigated by Deliceoğlu and Aydın [2]. Arun and Satheesh [1] analyzed the effects of aspect ratio and Reynolds number on flow structures in a rectangular cavity.

Most of the these studies in literature related to cavity flow are concerned with the square or rectangular cavity flows, although the cavities may be non-rectangular in applications. Gürcan & Bilgil [9], and Gürcan et al. [10] investigated bifurcations and eddy genesis mechanisms of Stokes flow in a sectorial cavity. Ertürk and Dursun [3] solved 2-D steady and driven skewed cavity flow of an incompressible fluid numerically for skew angles ranging between 15^o and 165^o. Ertürk and Gökçöl [4] studied 2-D,

Date: April 1, 2015 and, in revised form, September 14, 2015.
2010 *Mathematics Subject Classification.* 35Q35, 00A69.
Key words and phrases. Cavity, Bifurcation, Eddy, Flow Structure, Stagnation Point, Cavity Angle.

steady and incompressible flow inside a triangular driven cavity. A sequence of flow structures is illustrated by Gaskell et al. [7] for Stokes flow in a cylindrical cavity. Flow structures in different shaped cavities investigated by Ozalp et al. [15]. They showed effects of cavity shape on flow structure within the cavity in detail.

As can be seen from the literature survey given above and references therein, most of the studies on cavity flows are performed on cavity aspect ratio and speed ratio of moving lids. There is a need to investigate the effect of cavity angle on flow structure in annular wedge cavities. This is aim of this study.

2. Mathematical Formulation

We considered a two-dimensional creeping flow in an annular wedge cavity $r_1 \leq r \leq r_2, -\alpha \leq \theta \leq \alpha$ (Fig. 1). The side walls, $r = r_1$, $r = r_2$ are fixed. The boundaries $\theta = \alpha$ and $\theta = -\alpha$ are two moving lids, which translate with speeds U_1 and U_2 in the radial direction respectively. The equation for the stream function governing the two-

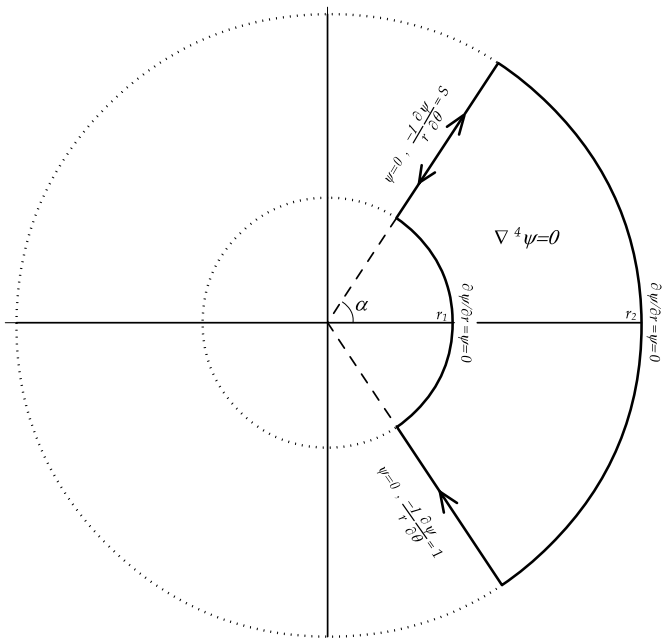

FIGURE 1. Geometry and boundary conditions for the lid driven cavity

dimensional steady flow of a viscous fluid is

$$\nabla^2\nabla^2\psi(r,\theta)=0, \tag{2.1}$$

where ∇^2 stands for the Laplace operator

$$\left(\frac{\partial^2}{\partial r^2}+\frac{1}{r}\frac{\partial}{\partial r}+\frac{1}{r^2}\frac{\partial^2}{\partial \theta^2}\right)^2 \tag{2.2}$$

in polar coordinates.

The derivatives of ψ give the velocity components:

$$u_r = -\frac{1}{r}\frac{\partial \psi}{\partial \theta} \quad , \quad u_\theta = \frac{\partial \psi}{\partial r} \ , \tag{2.3}$$

where u_r and u_θ are the radial and azimuthal components of velocity, respectively.

The streamfunction is constant (taken to be zero) on the boundaries

$$\psi(r_1,\theta) = \psi(r_2,\theta) = 0 \quad , \quad \psi(r,\pm\alpha) = 0 \ . \tag{2.4}$$

The ratio of the radii of the cylinders and speed ratio of the moving lids are our two control parameters which are defined by:

$$A = \frac{r_2}{r_1} \quad , \quad S = \frac{U_1}{U_2} \ . \tag{2.5}$$

In the plane polar coordinate system (r,θ), the other boundary conditions are

$$u_r(r,\alpha) = S \quad , \quad u_r(r,-\alpha) = 1 \ , \tag{2.6}$$

and on the side walls:

$$u_\theta(r_1,\theta) = u_\theta(r_2,\theta) = 0, \tag{2.7}$$

where we fixed $U_1 = S$ and $U_2 = 1$.

2.1. **Eigenfunction solution.** The general solution for the streamfunction can be written [13] in separable form as

$$\psi(r,\theta) = \sum_{-\infty}^{\infty} [E_n \sin(\lambda_n \theta) + F_n \cos(\lambda_n \theta)]\, \phi_1^{(n)}(r), \tag{2.8}$$

where

$$\phi_1^{(n)}(r,\lambda_n) = a_n r^{\lambda_n} + b_n r^{-\lambda_n} + c_n r^{2-\lambda_n} + d_n r^{2+\lambda_n} \ , \tag{2.9}$$

and λ_n are complex eigenvalues given by

$$\sin(\widehat{\lambda}_n) = \pm\beta\widehat{\lambda}_n \ , \tag{2.10}$$

where

$$\widehat{\lambda}_n = (i \ \log\frac{1}{A})\lambda_n \quad \text{and} \quad \beta = \frac{1}{2\log A}(A - \frac{1}{A}). \tag{2.11}$$

These complex eigenvalues are found via a Newton iteration procedure as described by Robbins & Smith [165], Fettis [5] and Khuri [13]; and values of the corresponding eigenvalues λ_n are given in Table 2.1.

The coefficients a_n, b_n, c_n and d_n have to be determined from the sidewall boundary conditions. These coefficients are given by Khuri [13].

The coefficients E_n and F_n in Eq. (2.8) have to be determined from the upper and the lower boundary conditions in (2,4) and (2,6). It is clear that the coefficients and the eigenvalues depends on S and A, respectively (see for details [55,99]).

Table 2.1: The first 30 roots of λ_n for $r_1 = 1, r_2 = 4$.

n	λ_n	n	λ_n
1	1.86054+2.99451i	11	3.75801+48.66728i
2	2.46101+7.70825i	12	3.82201+53.203498i
3	2.78163+12.30346i	13	3.88080+57.739178i
4	3.00270+16.86922i	14	3.93515+62.27442i
5	3.17170+21.42265i	15	3.98570+66.80932i
6	3.30856+25.96964i	16	4.03295+71.34393i
7	3.42358+30.51282i	17	4.07728+75.87830i
8	3.52277+35.05353i	18	4.11906+80.41247i
9	3.60998+39.59256i	19	4.15854+84.94646i
10	3.68778+44.13037i	20	4.19598+89.48031i

The infinite series thereby obtained are in practice truncated after N terms, i.e. the lower and upper summation limits are replaced by $-N$ and N, respectively. The convergence of the infinite series in (2.9) are necessary to determine the number N which assures that the truncated series is close enough to the infinite series.

3. RESULTS

We first analyzed flow structures and their bifurcations in a half-annular ring cavity. Then flow structures and their bifurcations in an annular wedge cavity wiht different cavity angle are investigated. Effects of the cavity angle on flow topology are revealed.

3.1. **Flow structures in a half-annular ring.** A half-annular ring cavity, $\alpha = \frac{\pi}{2}$ and $3.2 \leq r \leq 18$, consisting of two stationary side walls and both lids moving is considered; the boundary conditions and solution procedure are as given in section 2. As in Gürcan and Bilgil's work [9], mechanisms for eddy generation are examined via the emergence and the coalesce of corner-eedies or side-eddies as the aspect ratio is decreased; initially for single driven cavity, $S = 1$, and then for symmetric flow $S = -1$ and $S = 1$. For each case, the flow structures and eddy genesis mechanisms are illustrated in detail with figures.

3.1.1. *Bifurcations for a Single Lid-Driven Sectorial Cavity.* The aim of this section is to consider Stokes flow in a single lid driven annular cavity with three stationary walls (from Fig 1., $S = 0$ implies the top lid is stationary ; since the solutions obtained are independent of which lid is stationary and which one moves, to aid visualsation the flow patterns presented are for the case of a stationary bottom lid). Although the analytical solution of this problem was obtained by Khuri [13], he was not interested in the mechanism(s) of eddy generations.

In this case, the boundary conditions are defined as follows:

$$\psi(r_1,\theta) = \psi(r_2,\theta) = 0 \quad , \quad \psi(r,\pm\alpha) = 0 \tag{3.1}$$

and imposing the no-slip condition on all four walls gives,

$$u_\theta(r_1,\theta) = u_\theta(r_2,\theta) = 0 \tag{3.2}$$

$$u_r(r,\alpha) = 1 \quad , \quad u_r(r,-\alpha) = 0 \tag{3.3}$$

The values of the streamfunction and the radial velocity on top and bottom boundaries are given in Table 3.1. For different values of N in the infinite series in (2.8), the radial velocity on top and bottom boundaries are given in Table 3.2.

To investigate streamline bifurcations and hence a mechanism of eddy generation in this cavity, the aspect ratio was decreased, starting from $A = 18$ where the flow consist of a single main eddy and two smaller ones near the bottom corners (Fig. 2a). As A decreases it is observed that the corner eddies grow in size relative to the large central eddy, to meet each other on the bottom wall at a critical value of $A = 15.49$, see Fig. 2b. At this critical aspect ratio a new eddy is formed with a saddle point and a separatrix with streamfunction value $\psi = 0$. As A is decreased further this new eddy continues to grow (see Fig. 2c-d), the centers of two sub-eddies approach the saddle point and the center near the left-bottom of the cavity (say left center) coalesces with the saddle point to form a cusp bifurcation at $A = 12.05$. Hence these two critical points disappear and only the center near the right-bottom side of the cavity remains (say right center). In fact, at this critical aspect ratio the development of this second eddy is now complete as shown in Fig. 2e, $A = 11.10$. In this figure small corner eddies can be seen once again developing in each of the bottom corners. The process of eddy generation continues as the aspect ratio decreases(see Fig. 2f, where $A = 3.20$).

The same mechanism of eddy generation has similarly been reported by Gurcan [8,11] for the case of a rectangular cavity and Gurcan & Bilgil [9] for a sectorial cavity (for $\alpha = \frac{\pi}{4}$).

Table 3.1: The values of ψ and u_r on boundaries for $r_1 = 1$, $r_2 = 4$ and $N = 30$.

r	$\psi\left(r, \frac{\pi}{2}; 30\right)$	$\psi\left(r, -\frac{\pi}{2}; 30\right)$	$-\frac{1}{r}\frac{\partial \psi}{\partial \theta}\left(r, \frac{\pi}{2}; 30\right)$	$-\frac{1}{r}\frac{\partial \psi}{\partial \theta}\left(r, -\frac{\pi}{2}; 30\right)$
1.0	-9.6458E-17	-3.2719E-020	1.7708E-15	0
1.2	7.1537E-04	-7.8157E-13	0.8817E+01	-0.1332E-10
1.4	-1.1147E-03	3.0229E-12	0.1071E+01	0.3918E-10
1.6	-1.4256E-03	3.7842E-12	0.1122E+01	0.3750E-09
1.8	9.9134E-04	-3.8356E-12	0.9247E+00	-0.3135E-09
2.0	-1.8560E-03	4.8247E-12	0.1163E+01	0.5496E-09
2.2	-1.4157E-03	2.3535E-12	0.1123E+01	0.3588E-09
2.4	-1.9610E-03	3.1865E-12	0.1139E+01	0.3818E-09
2.6	-1.5174E-03	8.4531E-12	0.1047E+01	0.2580E-09
2.8	2.2270E-03	-3.4649E-12	0.9173E+00	-0.3142E-10
3.0	-1.7164E-04	-2.5217E-12	0.1036E+01	-0.4235E-09
3.2	1.6848E-03	2.0594E-11	0.9621E+00	0.5959E-09
3.4	-2.1931E-03	4.9270E-12	0.1170E+01	0.7111E-09
3.6	2.1211E-03	-1.3457E-11	0.9658E+00	-0.1104E-08
3.8	-4.6814E-05	2.9814E-11	0.1195E+01	-0.1758E-09
4.0	-3.9111E-16	2.0768E-19	0.6123E-15	0

Table 3.2: The values of u_r on boundaries for different N and $r_1 = 1$, $r_2 = 4$.

r	$-\frac{1}{r}\frac{\partial\psi}{\partial\theta}\left(r,\frac{\pi}{2};15\right)$	$-\frac{1}{r}\frac{\partial\psi}{\partial\theta}\left(r,-\frac{\pi}{2};15\right)$
1.0	0	0
1.6	0.9127	-0.1003-07
2.2	1.0922	0.8708E-08
2.8	1.0043	0.5807E-08
3.4	0.9439	-0.1674E-7
4.0	0	0
r	$-\frac{1}{r}\frac{\partial\psi}{\partial\theta}\left(r,\frac{\pi}{2};30\right)$	$-\frac{1}{r}\frac{\partial\psi}{\partial\theta}\left(r,-\frac{\pi}{2};30\right)$
1.0	0	0
1.6	1.1227	0.3750E-09
2.2	1.1236	0.3588E-09
2.8	0.9173	-0.3142E-10
3.4	1.1707	0.7111E-09
4.0	0	0
r	$-\frac{1}{r}\frac{\partial\psi}{\partial\theta}\left(r,\frac{\pi}{2};60\right)$	$-\frac{1}{r}\frac{\partial\psi}{\partial\theta}\left(r,-\frac{\pi}{2};60\right)$
1.0	0	0
1.6	1.0484	-0.2170E-10
2.2	1.0698	-0.9644E-11
2.8	1.0628	-0.2684E-10
3.4	0.8381	0.3904E-10
4.0	0	0
r	$-\frac{1}{r}\frac{\partial\psi}{\partial\theta}\left(r,\frac{\pi}{2};90\right)$	$-\frac{1}{r}\frac{\partial\psi}{\partial\theta}\left(r,-\frac{\pi}{2};90\right)$
1.0	0	0
1.6	1.0015	0.3599E-11
2.2	1.0003	-0.4064E-12
2.8	0.9996	-0.1018E-10
3.4	0.9928	-0.4382E-11
4.0	0	0

3.1.2. *Case* $S=-1$. In the case of lids moving in opposite directions with equal speeds, (i.e. $S=-1$), the flow structure is symmetrical about $\theta=0$ for all values of A. For large aspect ratios, a single eddy occupies the cavity, see Fig. 3a for $A=180$. As the aspect ratio is decreased from 180 there are four main stages in the development of the second and third eddies. In the first stage, a 'Pitchfork bifurcation appears at a critical value of $A_1=161.4$. Thus, two additional stagnation points are generated in the cavity, (see Fig. 3b where $A=130$).

As A is decreased further, the separatrix continues to grow and the second critical aspect ratio, $A_2=4.14$, is obtained at which two degenerate critical points appear on the two stationary side walls where side eddies are about to emerge as A is decreased further, see Fig. 3c-h.

In the third stage, at $A_3=3.56$, the heteroclinic connections coalesce with each other at the interior saddle point to produce four heteroclinic connections between the saddle point and the four separation points on the side walls, as shown in Fig. 3i (where $A=3.5$).

At this critical aspect ratio, A_3, there are now two complete eddies within the cavity and between them a third is about to be created. As A decreases, the sub-eddy center lying left of the saddle on $\theta=0$ approach the saddle point on $\theta=0$ and coalesce,

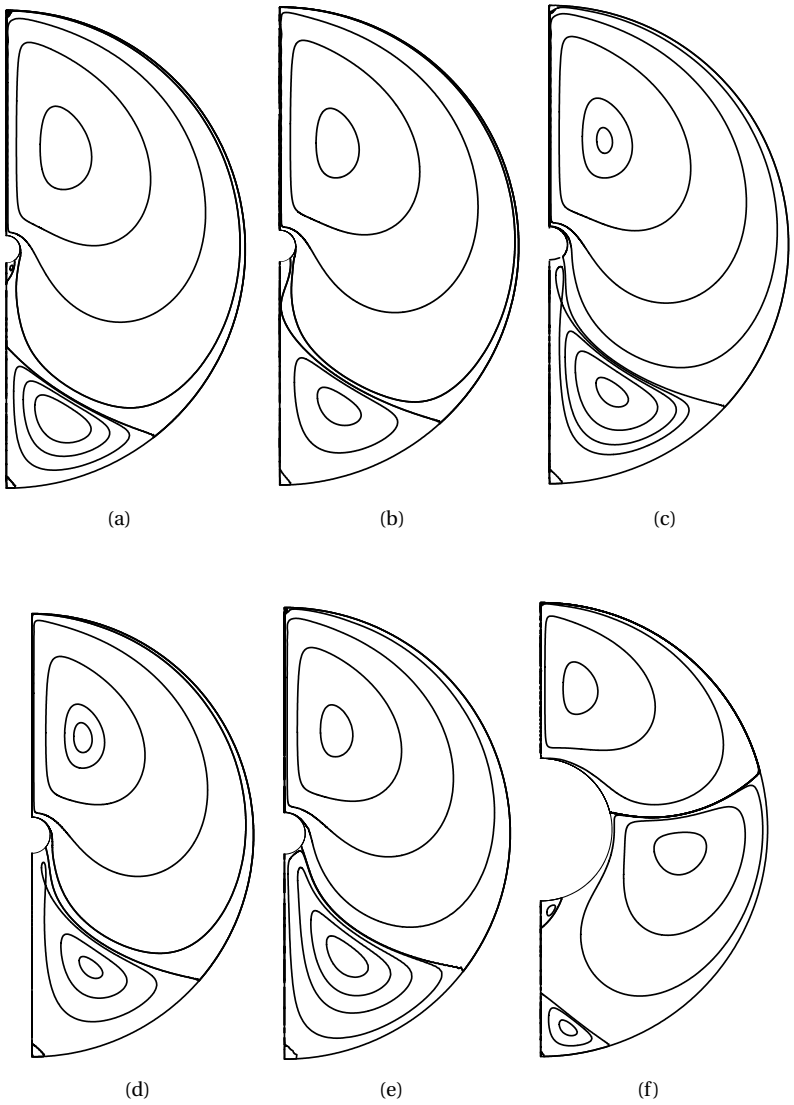

FIGURE 2. Eddy generation with decreasing A and S fixed at $S = 0$.
a) $A = 18.0$, b) $A = 15.49$, c) $A = 13.20$, d) $A = 12.50$, e) $A = 11.10$, f) $A = 3.20$

disappearing at $A_4 = 3.29$. This is a cusp (saddle-node) bifurcation. At this critical aspect ratio the formation of a third eddy, between the other two, is completed so that three eddies now occupy the cavity (Fig. 3j).

This is a mechanism for eddy generation in which one eddy becomes three. The number of complete eddies increases from 3 to 5 and 5 to 7 etc. via similar eddy genesis mechanism (see Fig. 3k-m).

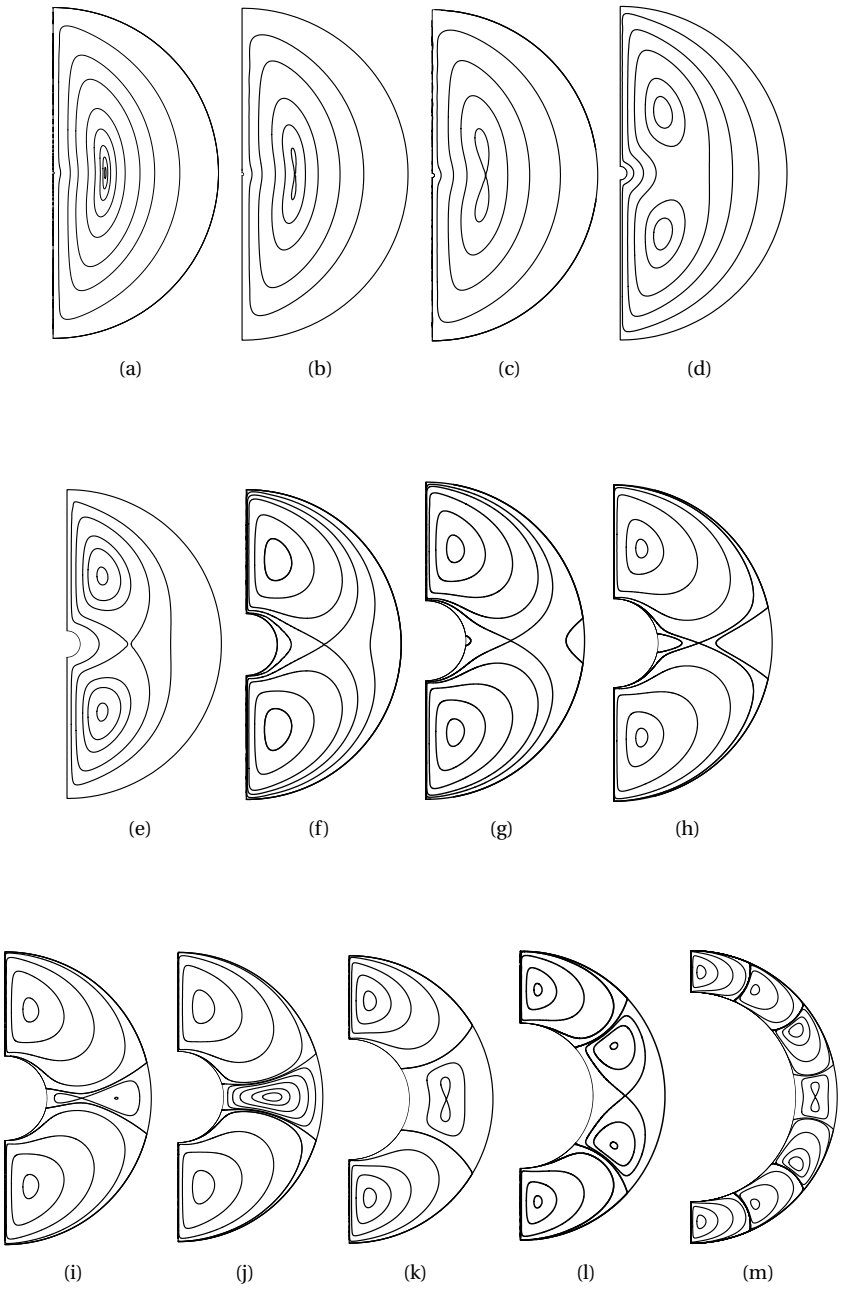

FIGURE 3. Eddy generation via the appearance of sides-eddies with decreasing A and S fixed at $S=-1$ for $\alpha=\frac{\pi}{2}$.
a) $A=180$, b) $A=130$, c) $A=90$, d) $A=25$, e) $A=12$, f) $A=5$, g) $A=4$, h) $A=3.6$, i) $A=3.5$, j) $A=3.2$, k) $A=2.4$, l) $A=2$, m) $A=1.4$

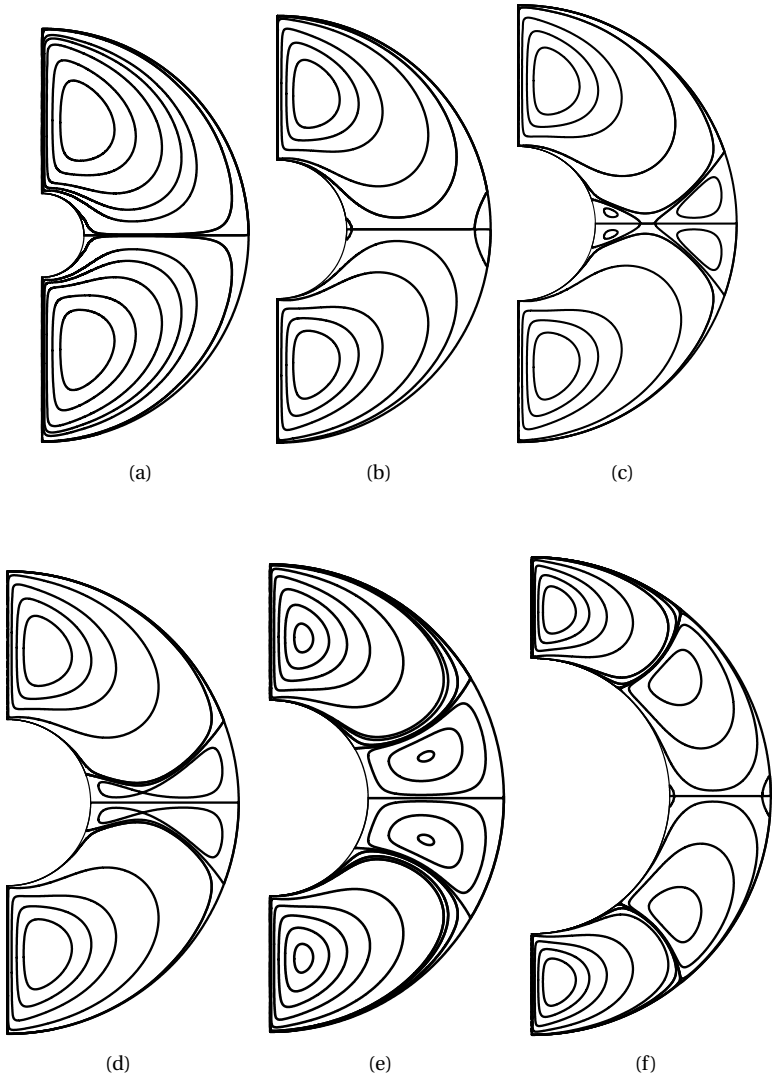

FIGURE 4. Eddy generation with decreasing A and S fixed at $S = 1$.
a) $A = 5$, b) $A = 3.1$, c) $A = 2.85$, d) $A = 2.8$, e) $A = 2.4$, f) $A = 1.74$

3.1.3. *Case* $S = 1$. In the case of lids moving in the same radial direction with equal speed, (i.e. $S = 1$), the flow structure is symmetric about $\theta = 0$ for all values of A. It is clear that the peripheral velocity is zero on $\theta = 0$.

For large aspect ratios, only two symmetric eddies occupy the cavity; see Fig. 4a for $A = 5$. As the aspect ratio is decreased from 5, there are three main stages in the simultaneously development of the third and fourth eddies. In the first stage, as A is decreased the first critical aspect ratio, $A_1 = 3.076$, is reached at which two degenerate critical points appear on each stationary sidewall; see Fig. 4b for $A = 3.10$. The side eddies approach each other as A is further decreased, such that, when $A_2 = 2.831$ is reached, they coalesce on $\theta = 0$. Thence a separatrix with a saddle point and two

centers (i.e. two sub-eddies) is seen in the cavity (see Fig.4c-d). As A decreases, the sub-eddy centers lying to the left of each of the saddles, approach the saddle point and coalesce, disappearing at $A_3 = 2.664$ which means that this is a cusp (saddle–node) bifurcation. Hence four fully developed eddies are now visible in the cavity (see Fig. 4e-f).

This is a mechanism that consists from three steps for eddy generation from two complete eddies to four. Firstly, side eddies born on each stationary sidewall. Secondly, these side eddies approach and coalesce each other to produce two reflected separatrices enclosing two sub-eddies. In the last step, the cusp bifurcation are seen on the each separatrix and there are now four complete eddies within the cavity. A similar mechanism in a sectorial cavity is given by Gürcan and Bilgil [9].

3.2. **Effect of the cavity angle on flow structures.** It is the aim of this section to track the various flow transformations arising in the cavity as α is gradually increased for $0 < \alpha < \pi$, and to expose the mechanisms by which new eddies emerge and develop within a sectorial cavity.

This work is, which to our knowledge, the first such study in the literature in terms of effect of cavity angle on flow structures and bifurcations.

For $S = 0, A = 3$ and $S = 1, A = 2$, the various flow transformations are tracked as α is increased and hence the means is identified by which new eddies appear and become fully developed.

3.2.1. *Case:* $S = 0$, $A = 3$. Solution of this problem is introduced in above section. For narrow cavity angle, a single eddy occupies the cavity; see Fig.5 for $\alpha = 15$, where the flow consist of a single main eddy and two smaller ones near the bottom corners.

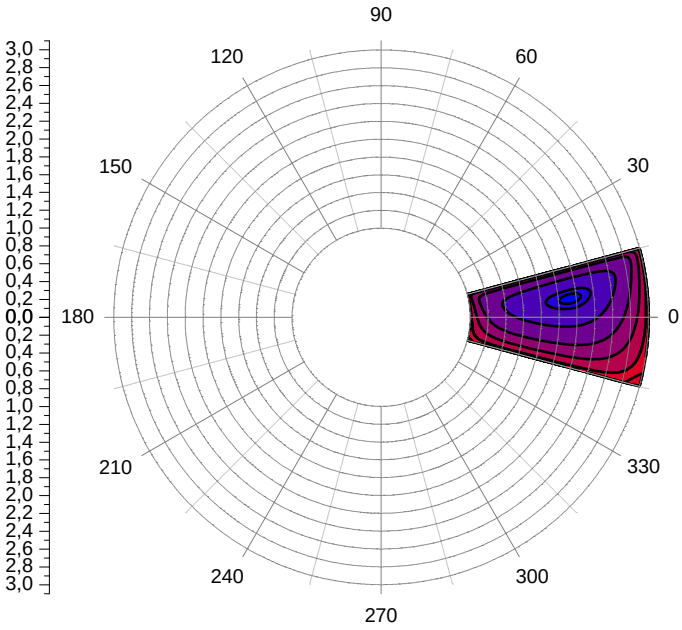

FIGURE 5. The cavity geometry and flow structure for $S = 0$, $A = 3$ and $\alpha = 15$.

As α increases it is observed that the corner eddies grow and meet each other on the bottom wall at a critical value of $\alpha = 47.31$, see Fig. 6a-d. At this critical cavity angle a new eddy is formed with a separatrix. As α is increased further this new eddy continues to grow and the centers of two sub-eddies approach the saddle point and the center near the left-bottom of the cavity coalesces with the saddle point to form a cusp bifurcation at $\alpha = 50.902$. Hence these two critical points disappear and only the center near the right-bottom side of the cavity remains see Fig. 6e-f. Hence the second eddy is completed in the cavity. As α increases the small corner eddies can be seen once again developing in each of the bottom corners. The process of eddy generation continues as the cavity angle increases (see Fig. 6g-p). It is seen that, as $\alpha \to \pi$, the number of completed eddy is five in the cavity for $A = 3$, see Fig.6p. It is clear that, in case of selecting smaller aspect ratio, the number of completed eddy will be more.

3.2.2. *Case:* $S = -1$, $A = 2$. In this special case the flow is symmetric about $\theta = 0$ for all values of α. When $5 \leq \alpha \leq 17.44$ (Fig. 7a-b) the flow in the cavity is in its simplest form: one single eddy with a centre-type stagnation point on $\theta = 0$. As α is gradually increased a sequence of flow transformations unfold, by which two additional eddies are generated in the cavity. For example, at $\alpha = 17.44$ the centre on $\theta = 0$ becomes a saddle point and two new centres appear (see Fig.7b where $\alpha = 22$). As α is increased further, the separatrix continues to grow and the second critical aspect angle is $\alpha = 48.24$, at which two degenerate critical points appear on the two side walls (see Fig. 7c-f).

As α increases, the side eddies expand and approach the saddle point on $\theta = 0$, and at $\alpha = 53.1$ coalesce with each other at the interior saddle point. At this critical cavity angle there are now two complete eddies within the cavity and between them a third is about to be created. As α is increased further, it seen that there are a separatrix between the two complete eddies (see Fig. 7g). As α increases, the sub-eddy center lying left of the saddle approach the saddle point on $\theta = 0$ and coalesce at $\alpha = 56.7$ to produce a centre. At this critical aspect ratio the development of the third eddy, between the other two, is complete so that three eddies now occupy the cavity (see Fig. 7h).

It can be seen from the above that there are four main stages in the development of the flow as the cavity aspect angle is increased: an interior saddle point appears; side eddies appear; the left side eddy and saddle point touch; and the interior substructure disappears.

This mechanism of eddy generation continues as the cavity angle increases (see Fig. 7i-r). It is seen that, as α is increased up to π, there are seven complete eddy and one separatrix in the cavity for $A = 2$ (see Fig. 7r). It is clear that, in the case of selecting smaller aspect ratio than $A = 2$, the number of complete eddy will be more.

In this study, derived from the one of the most important results, decreasing the aspect ratio (A) of cavity with increasing the cavity angle of flow structures cavity shows similar effects on the eddy genesis and their bifurcations.

ACKNOWLEDGEMENT

This research has been supported by Aksaray University Scientific Research Projects Coordination Unit. Project Number: 2014/012. H. Bilgil and Z. Dölek are grateful for this Financial support.

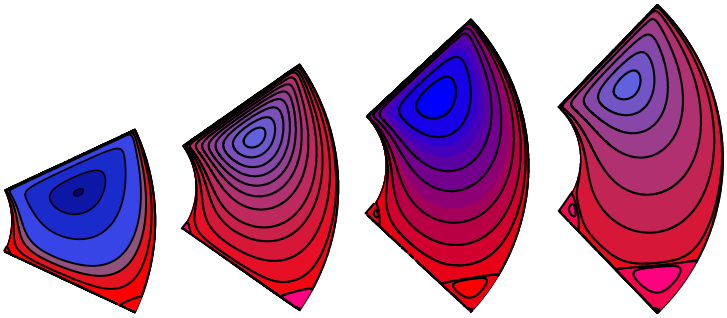

(a) (b) (c) (d)

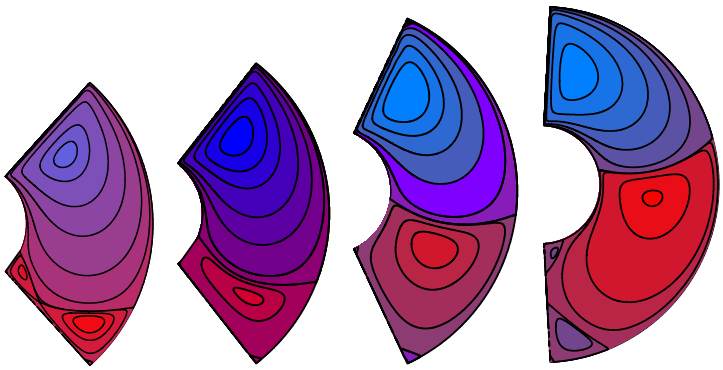

(e) (f) (g) (h)

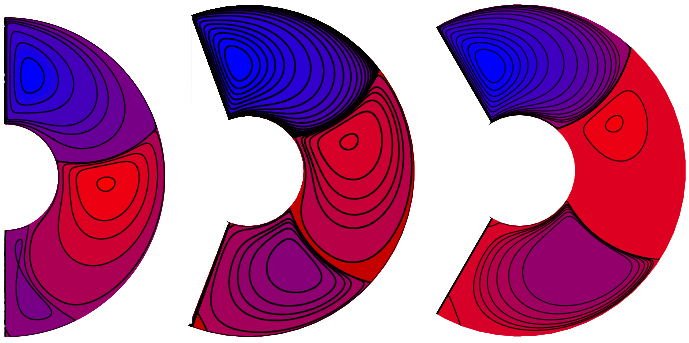

(i) (j) (k)

(Continue)

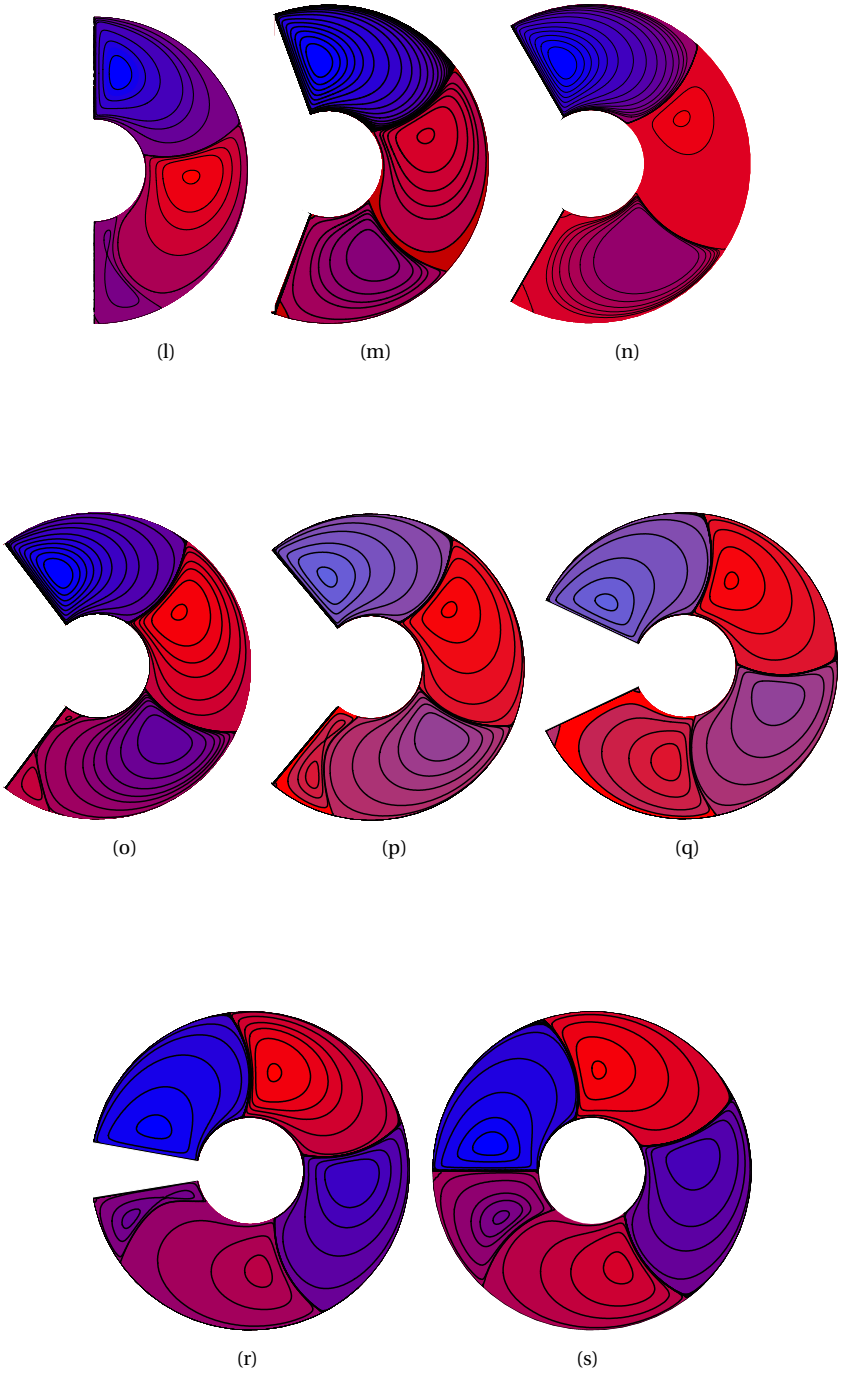

FIGURE 6. Eddy generation with increasing α for $S = 0$ and $A = 3$.
a) $\alpha = 25$, b) $\alpha = 35$, c) $\alpha = 43$, d) $\alpha = 46$, e) $\alpha = 48$, f) $\alpha = 52$, g) $\alpha = 65$, h) $\alpha = 87$, i) $\alpha = 90$, j) $\alpha = 110$, k) $\alpha = 120$, l) $\alpha = 127$, m) $\alpha = 130$, n) $\alpha = 155$, o) $\alpha = 170$, p) $\alpha \to 180$

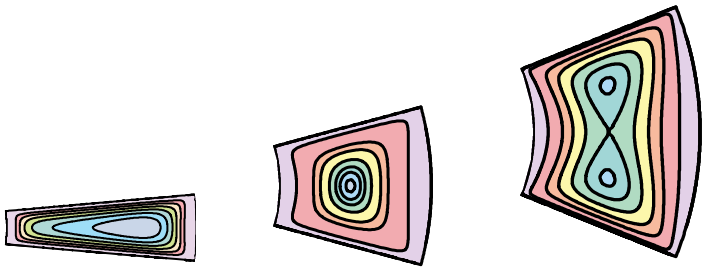

(a) (b) (c)

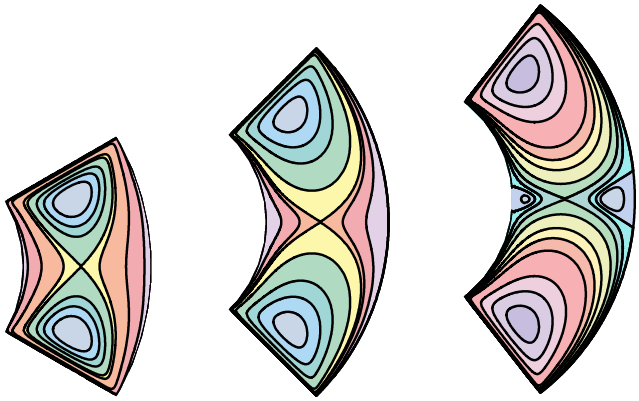

(d) (e) (f)

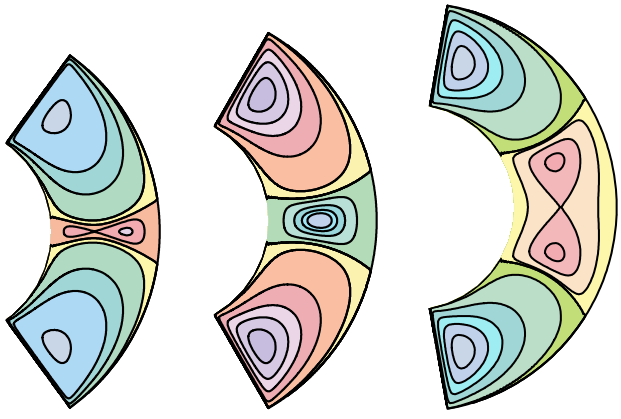

(g) (h) (i)

(Continue)

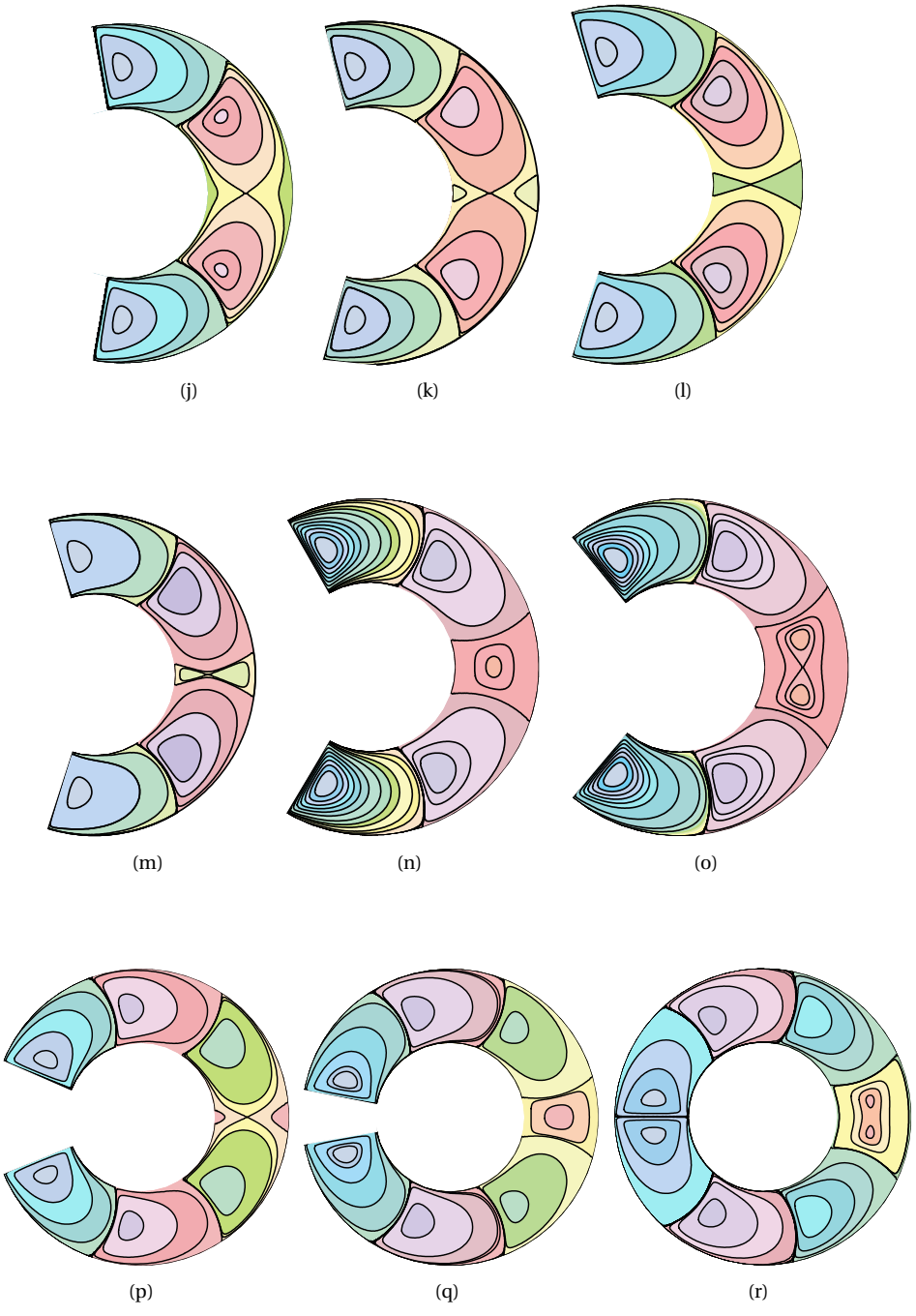

FIGURE 7. Eddy generation with increasing α for $S=-1$ and $A=4$. a) $\theta=5$, b) $\theta=15$, c) $\theta=22$, d) $\theta=30$, e) $\theta=45$, f) $\theta=52$, g) $\theta=54$, h) $\theta=60$, i) $\theta=80$, j) $\theta=100$, k) $\theta=105$, l) $\theta=106.76$, m) $\theta=107$, n) $\theta=120$, o) $\theta=130$, p) $\theta=158$, r) $\theta=170$, s) $\theta\to 180$

REFERENCES

[1] S. Arun, A. Satheesh, Analysis of flow behaviour in a two sided lid driven cavity using lattice boltzmann technique, Alexandria Engineering Journal, (2015), http://dx.doi.org/10.1016/j.aej.2015.06.005.

[2] A. Deliceoğlu, S.H. Aydın, Flow bifurcation and eddy genesis in an L-shaped cavity, Comput. Fluids 73 (2013), 24âĂŞ46.

[3] E. Erturk, B. Dursun, Numerical solution of 2-D steady incompressible flow in a driven skewed cavity, Z. Angew. Math. Mech. 87 (2007), 377âĂŞ392.

[4] E. Erturk, O. Gokcol, Fine grid numerical solutions of triangular cavity flow, Eur. Phys. J. Appl. Phys. 38 (2007), 97âĂŞ105.

[5] Fettis, H. E., Complex roots of $sinz = az, cosz = az$ and $coshz = az$, Math. of Comp. 30, 135 (1976), 541-545.

[6] Gaskell, P. H., Savage, M. D., Summers, J. L. and Thompson, H. M., Modeling and analysis of meniscus roll coating, J. Fluid Mech. 298 (1995), 113–137.

[7] P.H. Gaskell, M.D. Savage, M. Wilson, Flow structures in a half-filled annulus between rotating co-axial cylinders, J. Fluid Mech. 337 (1997), 263âĂŞ282.

[8] F. Gürcan, P.H. Gaskell, M.D. Savage, M. Wilson, Eddy genesis and transformation of Stokes flow in a double-lid-driven cavity, Proc. Inst. Mech. Eng. C 217, 3 (2003), 353âĂŞ364.

[9] Gürcan, F. and Bilgil, H., Bifurcations and eddy genesis of Stokes flow within a sectorial cavity, European Journal of Mechanics - B/Fluids. 39 (2013), 42-51.

[10] F. Gürcan, H. Bilgil, A. Åđahin, Bifurcations and eddy genesis of Stokes flow within a sectorial cavity PART II: Co-moving lids, European Journal of Mechanics - B/Fluids, (2015), dx.doi.org/10.1016/j.euromechflu.2015.02.008.

[11] Gürcan, F., Flow bifurcations in rectangular, lid-driven cavity flows. PhD Thesis, University of Leeds, 1996.

[12] Hellebrand H., Tape casting. In Materials Science and Technology–Processing of Ceramics, Part I, Vol. 17 A, ed. R. J. Brook. VCH, Weinheim, (1996), 189-260.

[13] S.A. Khuri, Biorthogonal series solution of stokes flow problems in sectorial regions, SIAM J. Appl. Math. 56, 1 (1996), 19âĂŞ39.

[14] Middleman S., Fundamentals of Polymer Processing, McGraw-Hill, New York, 1977.

[15] C. Ozalp, A. Pinarbasi, B. Sahin, Experimental measurement of flow past cavities of different shapes, Experimental Thermal and Fluid Science, 34, 5, (2010), 505-515.

[16] Robbins, C. I. and Smith, R. C. T., A table of roots of $Sinz = -z$, Phil. Mag. 39,7 (1948), 1005.

[17] Scholle M, Haas A, Aksel N, Thompson HM, Hewson RW, Gaskell PH, The effect of locally induced flow structure on global heat transfer for plane laminar shear flow, International Journal of Heat and Fluid Flow. 30, 2 (2009), 175-185.

AKSARAY UNIVERSITY, SCIENCE AND ART FACULTY, DEPARTMENT OF MATHEMATICS, AKSARAY-TURKEY
E-mail address: halis@gmail.com